Journal of
Materials Chemistry A

Materials for energy and sustainability

Accepted Manuscript

This article can be cited before page numbers have been issued, to do this please use: H. Ji, S. Niu, C. Zhang and X. Li, *J. Mater. Chem. A*, 2025, DOI: 10.1039/D5TA03829D.

ROYAL SOCIETY OF CHEMISTRY

rsc.li/materials-a

View Article Online
DOI: 10.1039/D5TA03829D

Redox-mediated bipolar hydrogen production and furoic acid electrosynthesis

Hyunjoon Ji,[ab] Siqi Niu,[a] Changkun Zhang[a] and Xianfeng Li*[a]*

[a]H. Ji, Dr S. Niu, Prof. C. Zhang, Prof. X. Li

Division of Energy Storage, Dalian National Laboratory for Clean Energy, Dalian Institute of Chemical Physics, Chinese Academy of Sciences, Dalian, 116023, China.

E-mail: zhangchk17@dicp.ac.cn, lixianfeng@dicp.ac.cn

[b]H. Ji

University of Chinese Academy of Sciences, Beijing 100049, China

Abstract

Hydrogen production coupling electrosynthesis is one of the promising strategies for upgrading traditional water electrolysis with reduced energy consumption. However, the coupling concept always needs a separate time-consuming discharge process to restore the mediator, thus lowering hydrogen productivity. Here, we propose a novel three-chamber-cell design to achieve continuous anodic and cathodic hydrogen production coupling furfural electrooxidation. Zinc or organic redox-active molecule mediators were applied to store and release energy and hydrogen independently on demand effectively. Simultaneous hydrogen production from two different chambers enabled furfural-hydrogen conversion efficiency of 184% with high energy storage flexibility. The three-chamber cell enabled the 2-furoic acid yield above 95%, while simultaneous cycling also yielded 2-furoic acid above 88% for 24 h. Our cell concept enhanced the time- and energy efficiency of furfural-hydrogen co-production.

Introduction

Hydrogen is the most abundant and lightest energy source on Earth, having no concerns about resource depletion since it can be produced by water electrolysis without leaving any harmful byproduct[1]. Green hydrogen production powered by renewables like solar and wind power has been getting growing attention as a solution to decarbonize traditional industries[2]. One of the technical challenges to industrial-scale water electrolysis is the cost burden originating from high water splitting voltage (>1.23 V) with sluggish oxygen evolution[3]. Research has been done on electrolyzer designs and non-noble metal-based catalysts to lower the high voltage and cost, thus reducing energy consumption[4]. One promising concept is combining hydrogen production with value-added electrosynthesis to generate hydrogen at a lower cell voltage and improve overall economic feasibility[5]. Various electrooxidations ranging from small molecules (e.g., glucose[6], furfural[7], and alcohols[8]) to more sophisticated organic synthesis (oxidative coupling,

View Article Online
DOI: 10.1039/D5TA03829D

dehydrogenation, oxygenation) have been proposed[5, 9]. Especially in terms of hydrogen production, biomass molecules containing aldehyde groups, such as formaldehyde[10], furfural[11], and hydroxymethylfurfural (HMF)[12], are considered suitable feedstocks due to their structural advantage of self-generating hydrogen. Combining the hydrogen evolution reaction (HER) with the biomass reaction enabled simultaneous hydrogen production from two different chambers[13].

When water electrolysis is coupled with redox couples, the cell can store the energy in redox couples and release it later for power generation and hydrogen production on demand[14]. Such a rechargeable battery concept allows operational flexibility by decoupling two half-cell reactions. For example, hydrazine or ammonia oxidation was coupled with zinc redox reactions to manage hydrazine, ammonia, and hydrogen at the same anode with the help of bifunctional catalysts[15]. However, the cell needs a time-consuming periodic discharge to restore the mediator, and the low economic value of the nitrogen gas product also remains less attractive. Coupling furfural redox cycling with nickel-based redox couple in a closed-battery concept produced both furoic acid and furfural alcohol, however, the nickel cathode was only used for redox reactions without any valuable products such as hydrogen[16]. Therefore, developing a more efficient cell concept equipped with both energy storage and hydrogen production is still necessary.

The present work proposed the combination of furfural oxidation and hydrogen production in an energy storage concept (Fig.1a). A three-chamber cell was assembled using redox mediations (zinc or other soluble organic redox-active molecules). 184% furfural-hydrogen conversion efficiency and 95% 2-furoic acid (2-FA) yield were reached during separate single-flow cycling, while simultaneous operation produced a 2-FA yield above 88% for 24h. Furthermore, using 7,8-dihydroxy-2-phenazinesulfonic acid (DHPS) mediator enabled electrolysis at 32% less energy consumption while maintaining the 2-FA yield above 92%. Our novel concept introduced a new possibility of time-efficient furfural-hydrogen co-production and electrochemical energy storage coupling.

Results

The working concept of our three-chamber cell is displayed in Fig. 1a-b. Furfural can be oxidized into the value-added furoic acid, simultaneously producing a half mole of hydrogen with the presence of Cu catalyst in chamber 1.[11a] The mediator chamber 2 was sandwiched between the furfural and the HER compartment (Fig. 1c). Zinc or organic redox-active molecules (7,8-dihydroxy-2-phenazinesulfonic acid (DHPS), benzo[*a*]hydroxyphenazine-7,8-carboxylic acid (BHPC)), having low redox potentials at -1.25 V, -0.9 V, and -0.78 V vs. SHE in alkaline solutions, respectively, were taken as mediator candidates (Fig. S1). $Zn(OH)_4^{2-}$ was reduced into solid Zn on the felt electrode during furfural oxidation at cell 1 (pairing chamber 1 and chamber 2) and the deposited Zn would be oxidized back to $Zn(OH)_4^{2-}$ while reducing hydrogen at cell 2 (pairing chamber 2 and chamber 3), enabling bipolar hydrogen production. Likewise, DHPS and BHPC can also be reduced in cell 1 and then released hydrogen when re-oxidized in cell 2, where the water-soluble phase of both reduced and oxidized states of molecules enables high-energy-density energy storage.

View Article Online
DOI: 10.1039/D5TA03829D

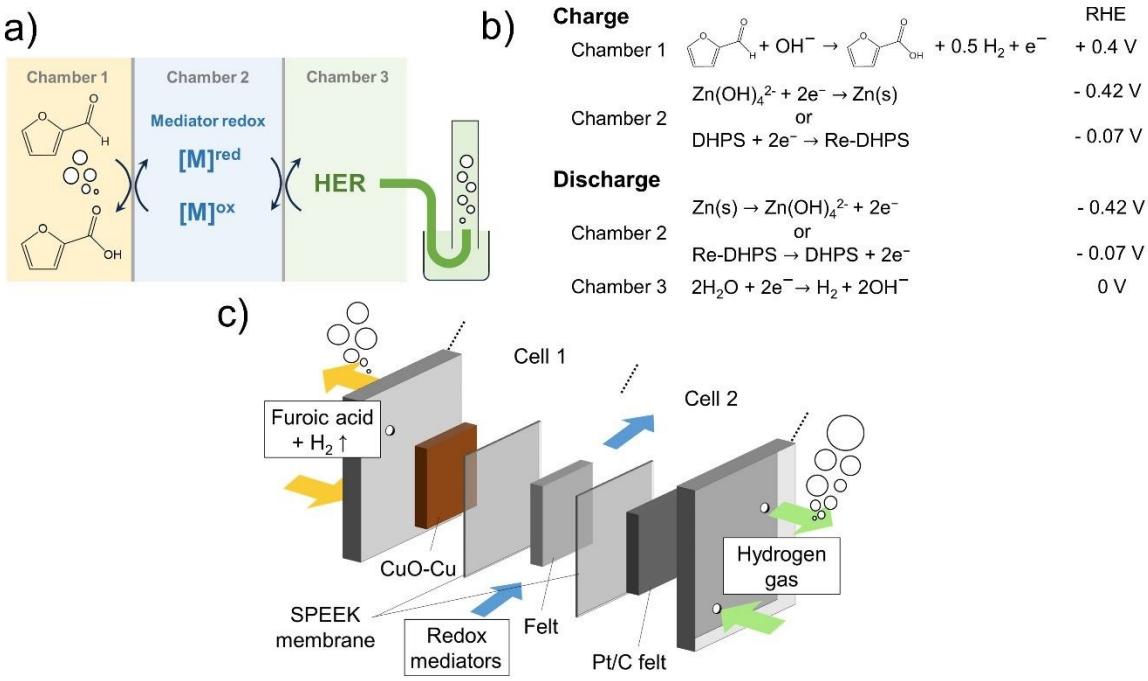

Fig. 1. Working concept of a three-compartment electroylsis cell

a) Reaction in different chambers and b) redox potential couplings in a three-chamber cell. Furfural oxidation (chamber 1) was coupled with zinc reduction (chamber 2) to form cell 1, while zinc oxidation (chamber 2) was combined with HER (chamber 3) to form cell 2. c) Schematic of a three-compartment cell assembly. Zinc mediator circulation was placed between the furfural oxidation and the HER chamber. Cu catalyst electrode, graphite felt, and Pt/C catalyst-coated felt were placed in chambers 1, 2, and 3, respectively. Sulfonated poly(ether ether ketone) (SPEEK) membranes separate each compartment to flow independently and keep the high purity of the products. Two channels were connected to cell 1 and cell 2, respectively, where the counter electrodes of both channels were connected to the zinc mediator compartment. DHPS-based electrolyte circulation was placed between electrochemical reduction in chamber 2 and a spontaneous chemical HER in chamber 3. The reduced state of DHPS (Re-DHPS) was re-oxidized back to DHPS when producing hydrogen.

Furfural electrooxidation

The furfural oxidation at Cu electrocatalysts was initially prepared by growing $Cu(OH)_2$ nanotube precursors on the Cu foam, which were then thermally treated at 500℃ in air or argon to attain CuO and Cu_2O, respectively. The $Cu(OH)_2$-Cu, CuO-Cu, and Cu_2O-Cu electrocatalysts were all obtained by electrochemically reducing the $Cu(OH)_2$, CuO, and Cu_2O, respectively. Scanning electron microscopy (SEM) revealed that the CuO-Cu catalyst showed crystal defects along nanotubes, whereas $Cu(OH)_2$-Cu revealed plain nanotubes, and Cu_2O-Cu showed nanotubes aggregated with each other (Fig. 2a and S2). X-ray diffraction (XRD) demonstrated that metallic Cu was the main phase for three catalysts, and a small amount of Cu_2O was found in CuO-Cu (Fig. 2b), which was also observed in transmission electron microscopy (TEM) (Fig. 2c). Auger electron spectroscopy (AES) Cu LMM revealed 1.9 eV distance between two main peaks, implying that metallic Cu and Cu_2O coexist (Fig. S3). X-ray photoelectron spectroscopy (XPS) indicated the existence of metallic Cu, Cu_2O (including Cu(OH), indicating Cu^+)[17], and even traces of CuO in all three samples (Fig. 2d). For XPS O1s, an additional high peak at around 532.9 eV at CuO-Cu,

View Article Online
DOI: 10.1039/D5TA03829D

corresponds to adsorbed oxygen species from moisture or organic adsorption (H_2O, C-O in Fig. 2e)[18]. XPS C1s spectra of CuO-Cu also revealed a higher portion of oxygen-bound adsorption (C-O, C=O, COO-), whereas Cu_2O-Cu and $Cu(OH)_2$-Cu adsorbed π-conjugated aromatics at higher binding energy (π→π* shake-up), indicating different adsorption behavior of CuO-Cu electrocatalyst (Fig. 2f). Double-layer capacitance measurement in 1 M KOH also revealed CuO-Cu showing much higher current and capacitance than Cu_2O-Cu and $Cu(OH)_2$-Cu, implying exceptional adsorption ability (Fig. S4). Vigorous oxygen removal during electrocatalyst preparation (electrochemical reduction) likely caused surface reconstruction to increase defects and contain a higher population of Cu sites of low coordination numbers than $Cu(OH)_2$-Cu and Cu_2O-Cu, resulting in strong adsorption energy[19].

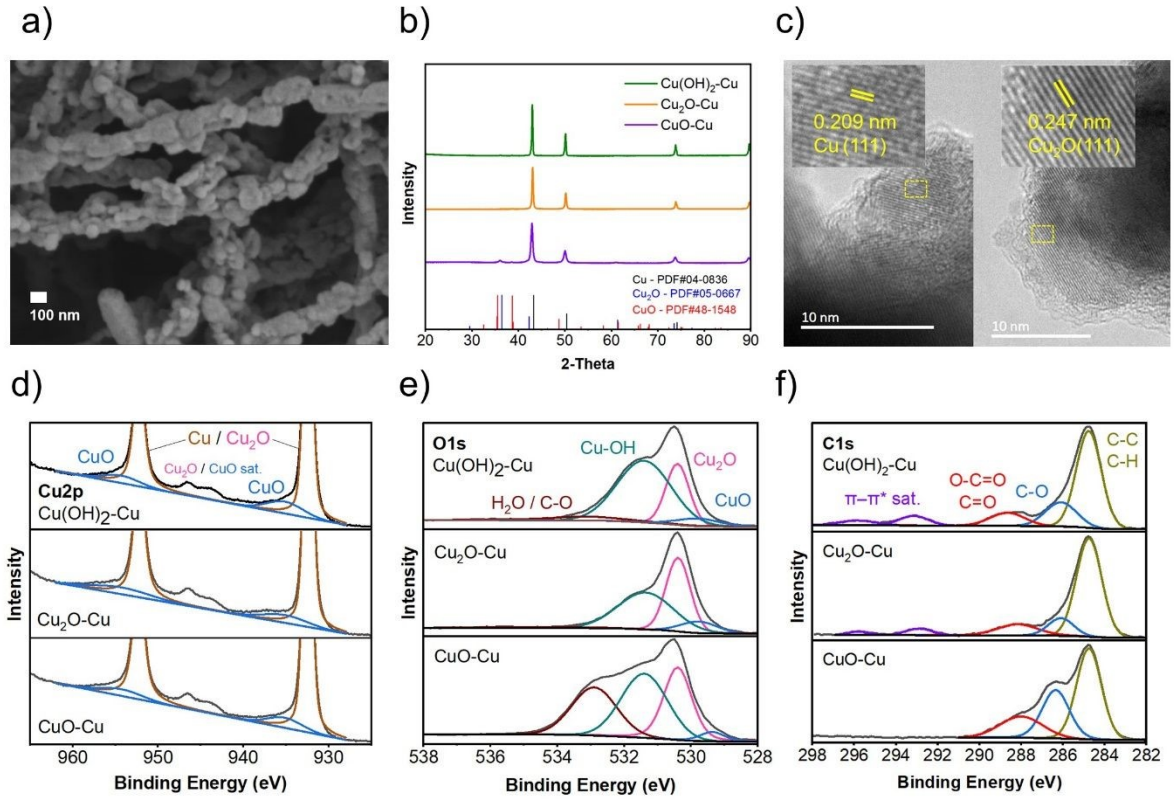

Fig. 2. Characterization of Cu electrocatalysts
a) SEM of CuO-Cu, b) XRD of $Cu(OH)_2$-Cu, Cu_2O-Cu, CuO-Cu electrocatalysts. c) TEM of CuO-Cu, XPS d) Cu2p, e) O1s, and f) C1s peak-fitting results of three electrocatalysts. CuO-Cu reveals an exceptionally high O1s peak at 532.9 eV.

The furfural oxidation performance at different catalysts was evaluated by the linear sweep voltammetry (LSV), and it is shown that a much higher current can be achieved when using CuO-Cu than $Cu(OH)_2$-Cu and Cu_2O-Cu (Fig. 3a). High current can be attributed to the richer population of defects and undercoordinated Cu sites, as mentioned above[19a, 20]. Furthermore, LSV current at different KOH concentrations increased along with the given potential, reaching the maximum current at 2 M [11a] (Fig. S5). Cu itself also began to oxidize when the potential was above 0.45 V vs. RHE, thus, the furfural chamber potential was fixed at 0.4 V vs. RHE for further experiments. When directly pairing furfural oxidation with

View Article Online
DOI: 10.1039/D5TA03829D

the hydrogen evolution reaction (HER) as an anode in a flow cell, furfural electrolyte was supplied as a continuous single-pass flow at an extremely slow flow rate of 1 ml min^{-1} to maximize the 2-FA yield (Fig. S6). Higher 2-FA yields were obtained along with the voltage increase (Fig. S7). Liquid chromatography-mass spectrometry (LC-MS) analysis revealed that at a cell voltage of 0.4 V using CuO-Cu, 2-FA was the main product, yielding 85 % with a trace of furfuryl alcohol by-product and 2-methylfuran (2-MF), due to the Cannizzaro disproportionation reaction (Fig. S8).

The stability of catalysts was then evaluated in a furfural-HER flow cell, which was maintained at a constant cell voltage of 0.4 V for 10 hours. It can be found that CuO-Cu maintained a current above 20 mA cm^{-2} for 10 hours compared with the rapid current decrease for $Cu(OH)_2$-Cu and Cu_2O-Cu based cells[11a, 13] (Fig. 3b). The current fluctuations can be attributed to more active hydrogen gas production on the catalyst surface. The surface of both $Cu(OH)_2$-Cu and Cu_2O-Cu quickly became dark-colored with a fast decline in current, which may have resulted from the severe Cu oxidation and organic deposition on the surface, evidenced by XPS and Raman analysis (Fig. 3c, S9). Surface hydroxyl groups (Cu-OH, 531.4 eV) of both $Cu(OH)_2$-Cu and Cu_2O-Cu also increased dramatically after 10 hours, while Cu_2O peak (530.4 eV) decreased, indicating changes in surface oxygen composition and its catalytic performance (Fig. 3d compared to previous Fig. 2e). In contrast, CuO-Cu maintained a relatively constant current with much less darkening than the other two substrates. The ratio of three O1s peaks (lattice oxygen of Cu_2O and CuO, surface hydroxyl groups, and adsorbed oxygen) remained almost the same after 10 hours, showing the robustness of the catalyst. The result also evidences the importance of surface defects in mitigating organic deposition, consistent with similar cases in carbon dioxide reduction on Cu[20-21]. During catalyst preparation, CuO took much longer to be electrochemically reduced than Cu_2O, indicating much more defects were made to improve the furfural adsorption. Therefore, CuO-Cu electrocatalyst was selected for the following steps. After 10 cycles, the actual hydrogen volume collected from the HER chamber reached 88 % of the theoretical hydrogen volume calculated from the charge capacity (Fig. S10). The efficiency loss could be attributed to overpotentials in cell components, HER catalytic activity, and the technical limitations of collecting small-sized hydrogen bubbles from the HER chamber. However, considering the simultaneously produced hydrogen at both furfural- and HER chambers, the average furfural-hydrogen conversion efficiency can reach 167 % (Fig. S10). Furfural-hydrogen conversion efficiency was calculated based on the sum of hydrogen collected from both cell 1 and cell 2, divided by the theoretical volume of hydrogen calculated from the charged capacity of cell 1.

$$\eta_{total} = (V_{cell1} + V_{cell2}) / V_{theo,\ cell1} \times 100$$

where V_{cell1} and V_{cell2} were the actual hydrogen volumes collected at cell 1 and cell 2, $V_{theo,\ cell1}$ was the theoretical volume of hydrogen calculated from the charged capacity of cell 1.

View Article Online
DOI: 10.1039/D5TA03829D

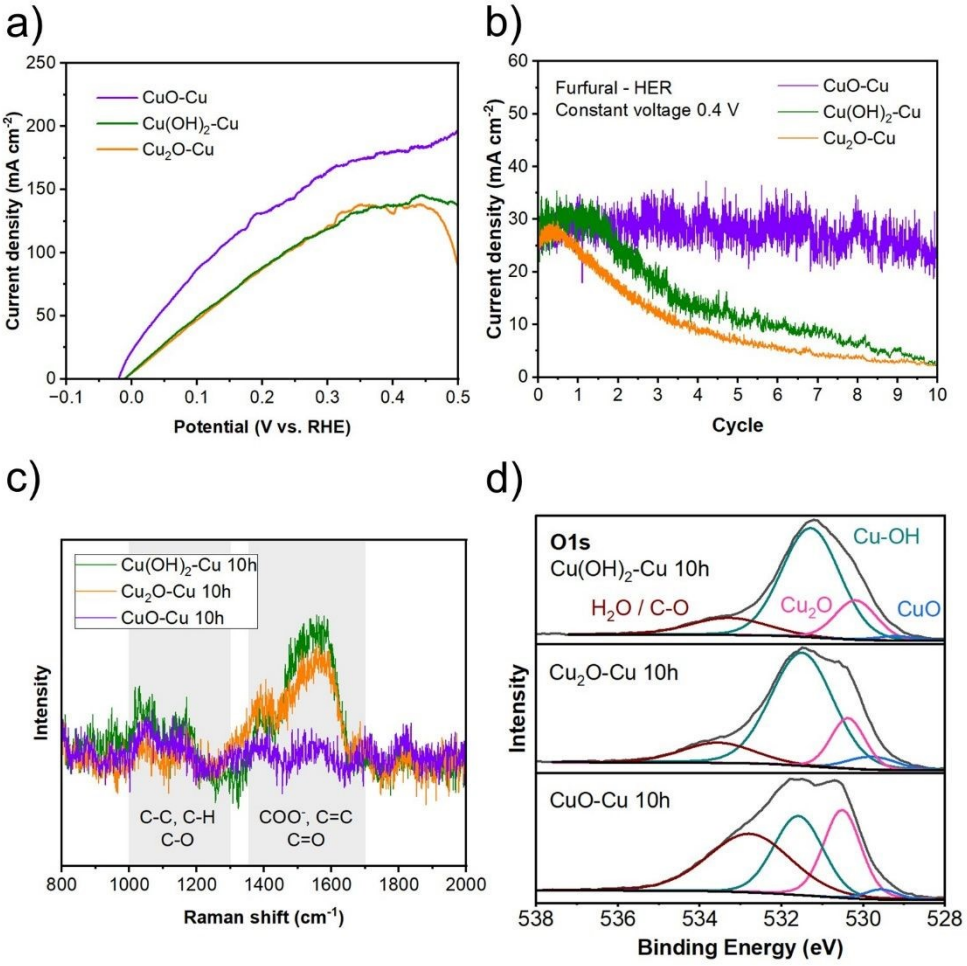

Fig. 3. Performance of Cu electrocatalysts
a) LSV curves of three electrocatalysts in 0.1M furfural and 2 M KOH. b) Stability of three electrocatalysts during 10 h single-pass flow electrolysis (Furfural-HER, constant voltage 0.4 V). Current densities using CuO-Cu decreased from 27 mA cm^{-2} to around 23 mA cm^{-2} after 10 h, whereas using $Cu(OH)_2$-Cu and Cu_2O-Cu reached around 2 mA cm^{-2}. c) Raman spectra of three electrocatalysts. Fewer aromatic absorptions were observed at CuO-Cu, which may partially explain the improved stability. d) XPS O1s peak-fitting results of three electrocatalysts after 10 h electrolysis. Three major O1s peaks of CuO-Cu were well maintained after the 10 h electrolysis.

Furfural electrooxidation coupling HER using zinc mediation

In the three-chamber cell (Fig. 1), 0.1 M furfural in 2 M KOH was given at a flow rate of 50 ml min^{-1} using recirculation, and cell 1 was fixed at a constant voltage of 0.8 V during electrolysis (Work model 1 in Fig. S11a). The maximum current density reached over 100 mA cm^{-2} and quickly decreased due to rapid furfural oxidation at a high flow rate (Fig. 4a). After cell 1 reached the cut-off current, cell 2 was discharged at a constant load of 1 ohm until reaching the cut-off 0 V for complete zinc oxidation. Cell 2 current was below 50 mA cm^{-2} and maintained a relatively flat curve like a zinc-air battery (Fig. S12). Ten batches of 10 ml furfural were oxidized in series. The average faradaic efficiency between cell 1 and cell 2 was 94%, and the 2-FA yield maintained an average of 90% (Fig. 4b). The average current was slightly reduced after 10 cycles, which could be attributed to the morphological degradation of the catalysts[11a]. Assuming cell 1 produced

View Article Online
DOI: 10.1039/D5TA03829D

the same amount of hydrogen as cell 2, the total hydrogen production from chamber 1 and chamber 3 increased after every cycle until reaching a limit of 10.4 ml (Fig. 4c), equivalent to around 152 % of the theoretical H_2 volume calculated from the capacity charged at cell 1.

Cell 1 and cell 2 can also work independently to enhance time efficiency by releasing hydrogen (cell 2) without stopping furfural oxidation (cell 1) (Work model 2 in Fig. S11b). As shown in Fig. 4d, the HER-discharge was started 'during' the cell 1 charge step, making the two cell operations partially overlap. Furfural electrolyte was supplied as a single-pass flow for continuous operation. For ten consecutive cycles, the cell 1 charge step maintained a constant current at around 30 mA cm^{-2} with current fluctuations due to hydrogen production on CuO-Cu electrode at a low flow rate. Cell 1 current was not disturbed by cell 2 current (current curves in Fig. 4d), showing the possibility of independent operations. 2-FA yields maintained above 95%, and the average furfural-hydrogen conversion efficiency was 184% (Fig. 4e). The average faradaic efficiency and furfural-hydrogen conversion efficiency were maintained similar to the previous batch experiment. To further evaluate the stability of the cells, a continuous simultaneous operation of cell 1 and cell 2 was also demonstrated for 24 hours (Work model 3 in Fig. S11c). Two cells maintained almost identical currents since zinc reduced in cell 1 was simultaneously oxidized in cell 2 (Fig. 4f). 2-FA yield was maintained above 88 % for 24 hours. Overall, the independence of the two cells in our three-chamber cell was verified, enabling time-efficient furfural and hydrogen production.

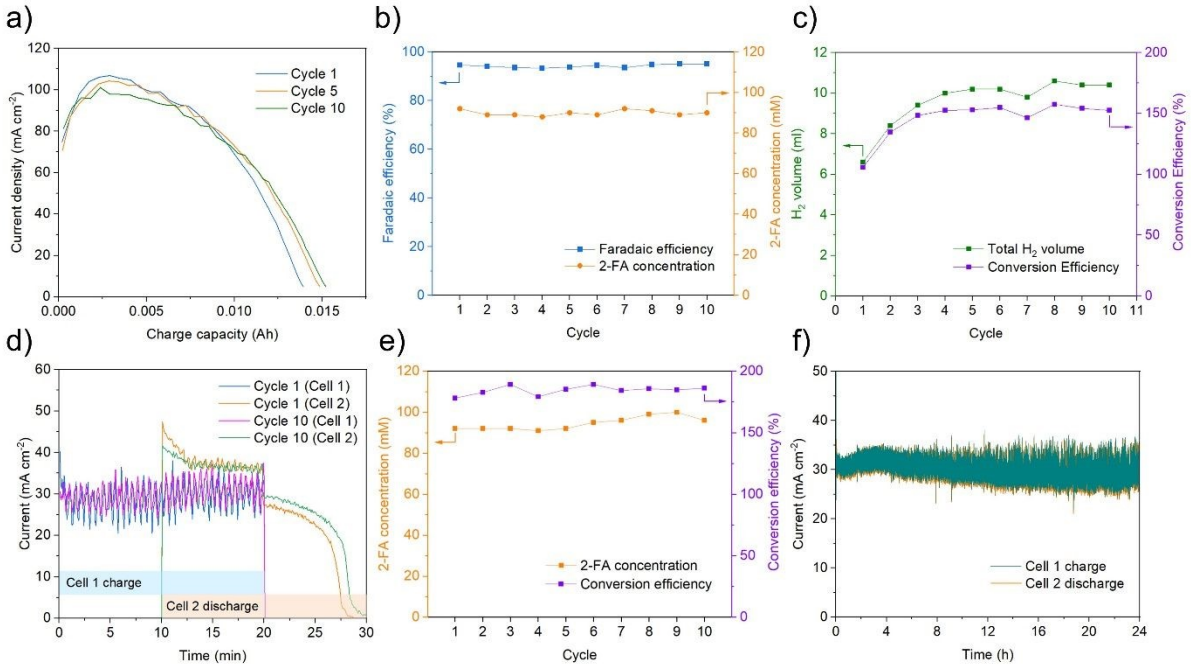

Fig. 4. Furfural-Zn-HER coupled electrolysis
a) Current profiles of cell 1 during furfural-Zn coupling using CuO-Cu as furfural catalyst. Cell 1 was given a constant cell voltage of 0.8 V immediately after the 10 ml furfural electrolyte was given as a batch. b) Cell performance of 10 cycles, faradaic efficiencies between cell 1 charge capacity and cell 2 discharge capacity (blue), and 2-FA product concentrations sampled from cell 1(orange). c) Total hydrogen volume, assuming cell 1 produced the same amount of hydrogen as cell 2 (green), and furfural-hydrogen conversion efficiencies (purple). d) Cell 1,2 current during the first and 10^{th} cycle (cell 2 discharge current was depicted as positive for comparison). Cell 2 started HER-discharge during the cell 1 charge step. Cell 1 current was not interrupted

View Article Online
DOI: 10.1039/D5TA03829D

when starting cell 2. Furfural electrolyte was supplied as a single-pass flow. e) 2-FA product concentrations sampled from cell 1 (orange) and furfural-hydrogen conversion efficiency (purple) over 10 cycles. f) Current during furfural-Zn-HER simultaneous 24 h cycling (cell 2 discharge current was depicted as positive for comparison)

Furfural electrooxidation coupling HER using soluble redox-active molecules mediation

Although zinc is advantageous in delivering a high discharge voltage due to its sufficiently low redox potential, it is always stored in a solid state, which limits its storage capacity. Zinc can also be replaced by soluble organic redox-active molecules to achieve higher energy-density hydrogen storage. As already shown in previous Fig. 1, the redox couples were reduced in a single electrochemical cell to oxidize furfural (cell 1), then sent to an external single-compartment cell assembled with Pt-coated felt (cell 2), where water was chemically oxidized to produce hydrogen, and the molecules were re-oxidized to the original state. Various organic redox-active molecules have been reported recently for energy storage applications[22]. Among them, DHPS and BHPC were considered as water-soluble redox couples (Fig. S1), where much higher energy densities can be expected than zinc by reaching maximum solubilities up to 1.8 M (DHPC) and 1.55 M (BHPC) in KOH solution[23]. Both DHPS and BHPC were reported to exhibit excellent capacity retention[23b, 23c]. Stable, long cycle life is expected when using DHPS in an inert, light-proof environment[24]. During electrolysis, the electrolyte half-cell potential (the potential measured against a reference electrode) of Re-DHPS quickly reached below HER potential around -0.83 V, causing spontaneous chemical HER when in contact with the Pt catalyst (Fig. S13). The Re-BHPC (reduced state of BHPC) can also react with water when the half-cell potential of electrolytes is below the HER potential. Both couplings indicated that spontaneous HER can be realized by involving electrolytes whose half-cell potential is below the HER potential. After HER, the potential turned back, enabling continuous circulation.

Furfural-DHPS cycling was performed by coupling 0.1 M furfural single-pass flow with 0.1 M DHPS circulation. A constant voltage of 0.45 V was maintained for 20 minutes each cycle, where the reduced state of DHPS (Re-DHPS) was pumped to an external Pt/C-cell for chemical HER discharge. Ten consecutive cycles yielded 92% 2-FA while maintaining the current almost the same (Fig. 5a and S14). The average furfural-hydrogen conversion efficiency reached around 184%, which was comparable to the furfural-HER two-electrode coupling (Fig. S15). Thanks to lower reduction potential, DHPS-mediated cycling consumed 0.55 kWh m^{-3} H_2, 32% less energy consumption per m^3 hydrogen than the previous Zn-mediated cycling (Fig. 5b). A zero-gap cell (furfural-HER) using a thinner 25 μm membrane (Alkymer, w-25) further reduced the energy consumption down to 0.37 kWh m^{-3} H_2, which was comparable to the previous publication[13] (Fig. S16). Continuous 24-hour electrolysis was performed using a higher storage capacity (DHPS 0.5 M, 1L) and a larger cell active area (36 cm^2), where the average 2-FA yield above 90 % was maintained (Fig. 5c, Supplementary Video 1). Current reached its maximum after around 10 hours, implying continuous activation of the catalyst over the large surface area during the electrolysis. Current decay afterwards can be attributed to organic deposition from furfural/furoic acid and morphological degradation. Cleaning with ethanol can help to partially remove surface deposition and restore the current and hydrogen production (Fig.

View Article Online
DOI: 10.1039/D5TA03829D

S17). Assuming an average of 7.5 ml min^{-1} hydrogen production from both chamber 1 and chamber 3 for 24 hours, a total of 20 L of hydrogen was achieved while synthesizing more than 1.3 L of 2-FA. Therefore, higher storage capacity can be expected when coupling liquid-phase redox molecules. Mitigating molecule crossover between chambers while minimizing the cell resistance remains a challenge. The DHPS-flowing chamber in the middle also requires compensation between cell resistance and structural complexity. Therefore, future research may focus on reducing the cell resistance and extending the reaction path to operate at faster flow rates, thereby maximizing both current density and 2-FA yield.

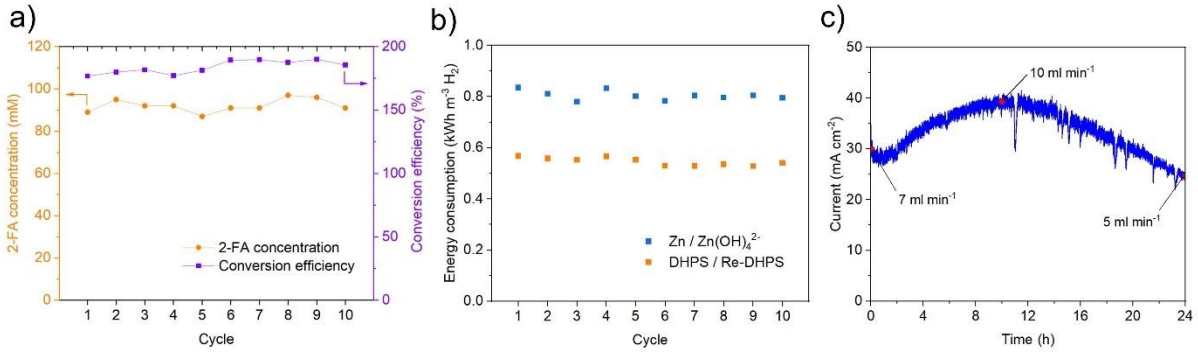

Fig. 5. Furfural-DHPS-HER coupled electrolysis
a) 2-FA yield and furfural-hydrogen conversion efficiency for 10 cycles. DHPS was reduced into Re-DHPS at cell 1 at a constant cell voltage of 0.45 V (furfural-DHPS) and re-oxidized in cell 2 (Pt/C-felt), chemically producing hydrogen. b) Energy consumption per m^{-3} H_2 compared with the previous Zn experiment in Fig. 4b. c) Cell 1 current and cell 2 hydrogen production rate during 24 h electrolysis at a higher storage capacity (DHPS 0.5 M, 1 L). Test conditions were scaled accordingly (cell active area 4 → 36 cm^{-2}, flow rate 1 → 9 ml min^{-1}) to maintain the same current density and 2-FA yield.

Conclusion

We have presented the concept of coupling 2-FA electrosynthesis and hydrogen production using zinc and DHPS mediation. A three-chamber cell was introduced to demonstrate separate or simultaneous charge-discharge cycling. Benefiting from hydrogen production at two different chambers and a highly stable oxide-derived CuO-Cu electrocatalyst, around 184% furfural-hydrogen conversion efficiency was reached. Changing zinc to DHPS allowed oxidation at lower energy consumption, with the possibility of higher storage capacity. Our novel concept introduced the new possibility of time-efficient furfural-hydrogen co-production.

Supporting Information

Supporting Information is available from the Wiley Online Library or from the authors.

Acknowledgements

View Article Online
DOI: 10.1039/D5TA03829D

The authors acknowledge financial support from Natural Science Foundation of China (No. 22209178 and 22279133), Liaoning Binhai Laboratory (No. LBLF202305 and LBLB202301), Energy Revolution S&T Program of Yulin Branch, the Dalian National Laboratory for Clean Energy, CAS (E411120705), and the LiaoNing Revitalization Talents Program (XLYC2403105). Prof. Xianfeng Li acknowledges the financial support from XPLORER PRIZE.

Conflict of Interest

The authors declare no conflict of interest.

References

[1] a) H. Jin, J. Xu, H. Liu, H. Shen, H. Yu, M. Jaroniec, Y. Zheng, S.-Z. Qiao, *Science Advances* **2023**, 9, eadi7755; b) J. Guo, Y. Zhang, A. Zavabeti, K. Chen, Y. Guo, G. Hu, X. Fan, G. K. Li, *Nature Communications* **2022**, 13, 5046; c) R. R. Beswick, A. M. Oliveira, Y. Yan, *ACS Energy Letters* **2021**, 6, 3167.

[2] a) K. de Kleijne, M. A. J. Huijbregts, F. Knobloch, R. van Zelm, J. P. Hilbers, H. de Coninck, S. V. Hanssen, *Nature Energy* **2024**, 9, 1139; b) T. Terlouw, C. Bauer, R. McKenna, M. Mazzotti, *Energy & Environmental Science* **2022**, 15, 3583; c) D. Hauglustaine, F. Paulot, W. Collins, R. Derwent, M. Sand, O. Boucher, *Communications Earth & Environment* **2022**, 3, 295.

[3] a) J. Wei, Y. Shao, J. Xu, F. Yin, Z. Li, H. Qian, Y. Wei, L. Chang, Y. Han, J. Li, L. Gan, *Nature Communications* **2024**, 15, 9012; b) J. Corbin, M. Jones, C. Lyu, A. Loh, Z. Zhang, Y. Zhu, X. Li, *RSC Advances* **2024**, 14, 6416.

[4] a) A. Hodges, A. L. Hoang, G. Tsekouras, K. Wagner, C.-Y. Lee, G. F. Swiegers, G. G. Wallace, *Nature Communications* **2022**, 13, 1304; b) S. Pan, H. Li, D. Liu, R. Huang, X. Pan, D. Ren, J. Li, M. Shakouri, Q. Zhang, M. Wang, C. Wei, L. Mai, B. Zhang, Y. Zhao, Z. Wang, M. Graetzel, X. Zhang, *Nature Communications* **2022**, 13, 2294; c) B. Rausch, M. D. Symes, L. Cronin, *Journal of the American Chemical Society* **2013**, 135, 13656; d) M. Chen, N. Kitiphatpiboon, C. Feng, A. Abudula, Y. Ma, G. Guan, *eScience* **2023**, 3, 100111.

[5] J. Li, H. Duan, *Chem* **2024**, 10, 3008.

[6] a) X. Lin, X. Xue, J. Du, *Journal of Materials Chemistry A* **2024**, 12, 32095; b) W.-J. Liu, Z. Xu, D. Zhao, X.-Q. Pan, H.-C. Li, X. Hu, Z.-Y. Fan, W.-K. Wang, G.-H. Zhao, S. Jin, G. W. Huber, H.-Q. Yu, *Nature Communications* **2020**, 11, 265.

[7] a) X. Liu, M. Albloushi, M. Galvin, C. W. Schroeder, Y. Wu, W. Li, *Green Chemistry* **2024**, 26, 11351; b) S. Kar, Q.-Q. Zhou, Y. Ben-David, D. Milstein, *Journal of the American Chemical Society* **2022**, 144, 1288.

[8] a) Z. Li, Y. Yan, S.-M. Xu, H. Zhou, M. Xu, L. Ma, M. Shao, X. Kong, B. Wang, L. Zheng, H. Duan, *Nature Communications* **2022**, 13, 147; b) D. Wang, P. Wang, S. Wang, Y.-H. Chen, H. Zhang, A. Lei, *Nature Communications* **2019**, 10, 2796; c) M. Huang, C. Cao, L. Liu, W. Wei, Q.-L. Zhu, Z. Huang, *eScience* **2023**, 3, 100118.

[9] a) H. Ji, Z. Zhao, C. Zhang, X. Li, *Chemical Science* **2024**, 15, 13185; b) B. Garlyyev, S. Xue, J. Fichtner, A. S. Bandarenka, C. Andronescu, *ChemSusChem* **2020**, 13, 2513; c) H. Sun, X. Xu, L. Fei, W. Zhou, Z. Shao, *Advanced Energy Materials* **2024**, 14, 2401242.

[10] G. Li, G. Han, L. Wang, X. Cui, N. K. Moehring, P. R. Kidambi, D. E. Jiang, Y. Sun, *Nat Commun* **2023**, 14, 525.

[11] a) T. Wang, Z. Huang, T. Liu, L. Tao, J. Tian, K. Gu, X. Wei, P. Zhou, L. Gan, S. Du, Y. Zou, R. Chen, Y. Li, X. Z. Fu, S. Wang, *Angew Chem Int Ed Engl* **2022**, 61, e202115636; b) H. Liu, N. Agrawal, A. Ganguly, Y. Chen, J. Lee, J. Yu, W. Huang, M. Mba Wright, M. J. Janik, W. Li, *Energy & Environmental Science* **2022**, 15, 4175.

[12] G. Fu, X. Kang, Y. Zhang, Y. Guo, Z. Li, J. Liu, L. Wang, J. Zhang, X.-Z. Fu, J.-L. Luo, *Nature Communications* **2023**, 14, 8395.

[13] T. Wang, L. Tao, X. Zhu, C. Chen, W. Chen, S. Du, Y. Zhou, B. Zhou, D. Wang, C. Xie, P. Long, W.

View Article Online
DOI: 10.1039/D5TA03829D

Li, Y. Wang, R. Chen, Y. Zou, X.-Z. Fu, Y. Li, X. Duan, S. Wang, *Nature Catalysis* **2021**, 5, 66.
[14] C. Chen, Z. Fu, F. Qi, Y. Chen, G. Meng, Z. Chang, F. Kong, L. Zhu, H. Tian, H. Huang, X. Cui, J. Shi, *Angew Chem Int Ed Engl* **2022**, 61, e202207226.
[15] a) Y. Feng, Q. Shi, J. Lin, E. Chai, X. Zhang, Z. Liu, L. Jiao, Y. Wang, *Adv Mater* **2022**, 34, e2207747; b) Y. Feng, L. Huang, Z. Xiao, X. Zhuang, T. S. Aslam, X. Zhang, Y.-X. Tan, Y. Wang, *Journal of the American Chemical Society* **2024**, 146, 7771.
[16] J. Li, K. Ji, B. Li, M. Xu, Y. Wang, H. Zhou, Q. Shi, H. Duan, *Angew Chem Int Ed Engl* **2023**, 62, e202304852.
[17] M. Yang, Y. Li, C.-L. Dong, S. Li, L. Xu, W. Chen, J. Wu, Y. Lu, Y. Pan, Y. Wu, Y. Luo, Y.-C. Huang, S. Wang, Y. Zou, *Advanced Materials* **2023**, 35, 2304203.
[18] E. Gioria, S. Li, A. Mazheika, R. Naumann d'Alnoncourt, A. Thomas, F. Rosowski, *Angewandte Chemie International Edition* **2023**, 62, e202217888.
[19] a) C. Long, X. Liu, K. Wan, Y. Jiang, P. An, C. Yang, G. Wu, W. Wang, J. Guo, L. Li, K. Pang, Q. Li, C. Cui, S. Liu, T. Tan, Z. Tang, *Science Advances* **2023**, 9, eadi6119; b) P. Hauke, T. Merzdorf, M. Klingenhof, P. Strasser, *Nature Communications* **2023**, 14, 4708.
[20] K. Xiang, F. Zhu, Y. Liu, Y. Pan, X. Wang, X. Yan, H. Liu, *Electrochemistry Communications* **2019**, 102, 72.
[21] J.-W. DuanMu, Z.-Z. Wu, F.-Y. Gao, P.-P. Yang, Z.-Z. Niu, Y.-C. Zhang, L.-P. Chi, M.-R. Gao, *Precision Chemistry* **2024**, 2, 151.
[22] a) Z. Zhao, X. Liu, M. Zhang, L. Zhang, C. Zhang, X. Li, G. Yu, *Chemical Society Reviews* **2023**, 52, 6031; b) Z. Zhao, T. Li, C. Zhang, M. Zhang, S. Li, X. Li, *Nature Sustainability* **2024**, 7, 1273; c) M. Zhang, C. Mu, T. Li, C. Zhang, X. Li, *Advanced Energy Materials* n/a, 2404813; d) J. Zhang, Y. Zhang, J. Fu, X. Li, C. Zhang, *Electron* **2024**, 2, e57.
[23] a) F. Zhang, H. Zhang, M. Salla, N. Qin, M. Gao, Y. Ji, S. Huang, S. Wu, R. Zhang, Z. Lu, Q. Wang, *J Am Chem Soc* **2021**, 143, 223; b) C. Wang, X. Li, B. Yu, Y. Wang, Z. Yang, H. Wang, H. Lin, J. Ma, G. Li, Z. Jin, *ACS Energy Letters* **2020**, 5, 411; c) A. Hollas, X. Wei, V. Murugesan, Z. Nie, B. Li, D. Reed, J. Liu, V. Sprenkle, W. Wang, *Nature Energy* **2018**, 3, 508.
[24] X. Xu, F. Sun, W. Tian, C. Zhang, X. Li, *Small Methods* n/a, 2500477.

View Article Online
DOI: 10.1039/D5TA03829D

ARTICLE

Redox-mediated bipolar hydrogen production and furoic acid electrosynthesis†

Received 00th January 20xx,
Accepted 00th January 20xx

DOI: 10.1039/x0xx00000x

Hyunjoon Ji,[ab] Siqi Niu [a] , Changkun Zhang *[a] and Xianfeng Li*[a]

Data availability

All data supporting this article are available as part of the article and its ESI file.

[a.] *Dalian Institute of Chemical Physics, Chinese Academy of Sciences, Zhongshan Road 457, Dalian 116023, P. R. China. E-mail: zhangchk17@dicp.ac.cn, lixianfeng@dicp.ac.cn*
[b.] *University of Chinese Academy of Sciences, Beijing 100049, P. R. China*
†Electronic Supplementary Information (ESI) available: See DOI: 10.1039/x0xx00000x